Communication

Dynamics and Efficiency of DNA Hole Transport via Alternating AT versus Poly(A) Sequences

Frederick D. Lewis, Pierre Daublain, Boiko Cohen, Josh Vura-Weis, Vladimir Shafirovich, and Michael R. Wasielewski

J. Am. Chem. Soc., **2007**, 129 (49), 15130-15131 • DOI: 10.1021/ja076876o

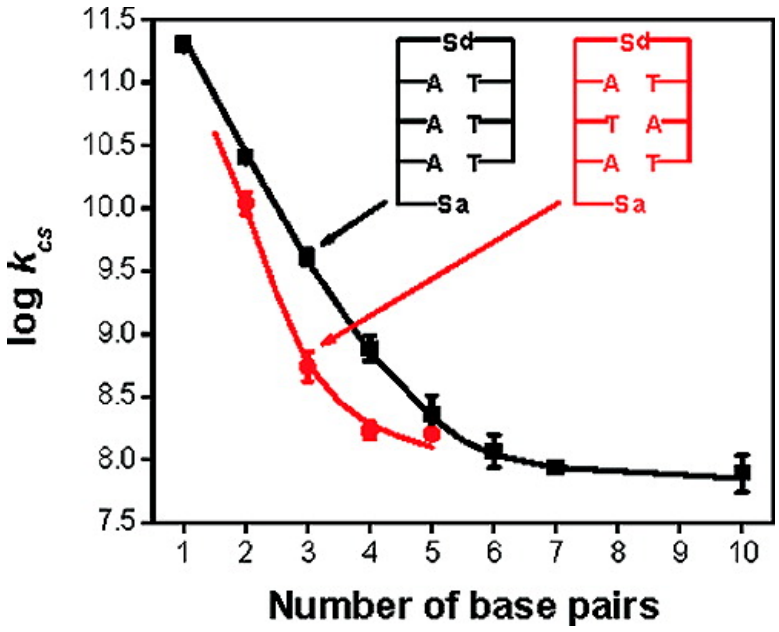

More About This Article

Additional resources and features associated with this article are available within the HTML version:

- Supporting Information
- Access to high resolution figures
- Links to articles and content related to this article
- Copyright permission to reproduce figures and/or text from this article

View the Full Text HTML

J|A|C|S COMMUNICATIONS

Published on Web 11/17/2007

Dynamics and Efficiency of DNA Hole Transport via Alternating AT versus Poly(A) Sequences

Frederick D. Lewis,*,† Pierre Daublain,† Boiko Cohen,† Josh Vura-Weis,† Vladimir Shafirovich,‡ and Michael R. Wasielewski*,†

Department of Chemistry, Northwestern University, Evanston, Illinois 60208, and Department of Chemistry, New York University, New York, New York 10003

Received September 11, 2007; E-mail: fdl@northwestern.edu; m-wasielewski@northwestern.edu

Understanding the base sequence dependence of photoinduced charge transfer and hole transport processes in DNA continues to provide challenges for both experiment and theory.[1] Much of our current understanding of these processes is based on the use of poly(A) base sequences (A-tracts) to separate guanine hole traps or organic chromophores serving as hole donors and acceptors.[2−7] Alternating poly(AT) sequences have received less attention. Theories for hole transport based on either localized or delocalized holes indicate a substantial advantage for hole transport via poly(A) versus poly(AT) sequences.[8] However, the available experimental evidence indicates that hole transport across poly(A) sequences is only modestly more efficient than across poly(AT) sequences.[2] No direct measurements of the dynamics of charge transfer across poly(AT) sequences have been reported.

We report here the results of our investigation of the dynamics and efficiencies of photoinduced charge separation across AT, ATA, ATAT, and ATATA base pair (bp) sequences in synthetic capped hairpins possessing a stilbenedicarboxamide (Sa) capping group and a stilbenediether (Sd) hairpin linker (Chart 1, **nAT**). Comparison of these results with our recently published data for charge separation in poly(A) sequences (Chart 1, **nA**)[6,7] reveals the occurrence of significantly slower and less efficient charge separation for poly(AT) versus poly(A) sequences at short distances (2−4 bp). However, at longer distances, the kinetics and efficiencies for charge separation in poly(AT) and poly(A) sequences become weakly distance-dependent and are similar in magnitude.

The Sa-capped hairpins **2AT**−**5AT**, **10A**, and $\mathbf{H_1}$−$\mathbf{H_3}$ were prepared by the procedures previously employed for the synthesis of **1A**−**7A**.[6,7] The long wavelength UV (>300 nm) absorption and fluorescence band shapes of the **nAT**, **nA**, and $\mathbf{H}_n$ series are similar (Figures S1−S5); however, the extinction coefficients of the base pair domains are larger and the maxima are red-shifted for the **nAT** versus **nA** sequences. Fluorescence quantum yields obtained using 340 nm excitation which selectively excites Sa are reported in Table 1. The values of Φ_f for the **nAT** series are larger than the corresponding values for the **nA** series for $n > 1$ (Figure 1a) and indicate a weaker fluorescence quenching due to hole transfer in the **nAT** series. Fluorescence decays for **3-5AT** can be fit as either double or triple exponentials (Table S1). As previously reported for **3A**−**7A**, long-lived components (1.2−2.0 ns) are attributed to delayed fluorescence resulting from charge recombination (Scheme 1).[7]

Femtosecond (fs) time-resolved transient absorption spectra in aqueous solution were obtained using 350 nm excitation (providing selective excitation of Sa) from a Ti-sapphire-based system having a time resolution of ca. 180 fs, a spectral range of 425−850 nm, and a time window of 0−6 ns.[6] Transient spectra for hairpin **2AT**−**5AT** are shown in Figures 2 and S6−S8. Laser excitation initially yields a single band with a maximum at 575 nm attributed to the locally excited ^{1}Sa* singlet state (Figure S9). Initial growth of a 525 nm shoulder over 50−100 ps is attributed to the formation of $Sa^{-\bullet}$ (Scheme 1), which has a 525/575 nm band intensity ratio of ca. 0.4. $A^{+\bullet}$ does not absorb in this wavelength region. Continued growth of the 525/575 nm band intensity ratio (inset in Figure 2) is attributed to formation of $Sd^{+\bullet}$ which has an absorption maximum at 535 nm.[7] Plots of the time dependence of the 525/575 nm band intensity ratio for **3AT**−**5AT** have fast and slow components attributed to hole injection (τ_i) and hole arrival at Sd (τ_a), respectively (Scheme 1). Values of τ_a for **2AT**−**5AT** are reported

Chart 1. Structures of the Sa−Sd Hairpins **1A**−**7A**, **10A**, **2AT**−**5AT**, and of the Sa End-Capped Hairpins $\mathbf{H_1}$−$\mathbf{H_3}$

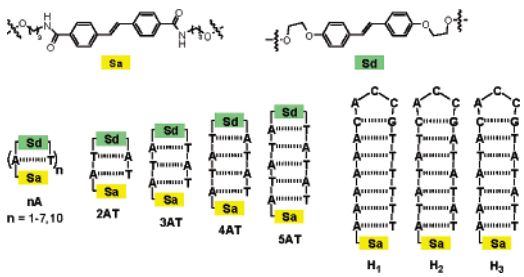

Table 1. Fluorescence Quantum Yields, Hole Arrival Times, Hole Trapping Quantum Yields, and Hole Injection Times for Sa−Sd Hairpins **1A**−**7A**, **10A**, and **2AT**−**5AT**, and for Sa Models $\mathbf{H_1}$−$\mathbf{H_3}$[a]

hairpin	Φ_f[b]	τ_a, ns[c]	Φ_{cs}[d]
1A	0.0080	0.0051 ± 0.0012	1
2A	0.029	0.039 ± 0.004	0.8 ± 0.1
3A	0.068	0.25 ± 0.03	0.5 ± 0.1
4A	0.15	1.3 ± 0.3	0.23 ± 0.01
5A		4.5 ± 1.5	0.10 ± 0.05
6A	0.23	9 ± 4	0.09 ± 0.03
7A	0.25	12 ± 4	0.06 ± 0.03
10A	0.24	13 ± 4	
2AT	0.047	0.09 ± 0.02	0.5 ± 0.1
3AT	0.21	1.9 ± 0.6	0.12 ± 0.02
4AT	0.25	6 ± 1	0.03 ± 0.02
5AT	0.26	6 ± 2	0.02 ± 0.01
		τ_i, ps[e]	
$\mathbf{H_1}$	0.24	50 ± 10	
$\mathbf{H_2}$	0.28	110 ± 20	
$\mathbf{H_3}$	0.24	58 ± 6	

[a] Data in aqueous solution (standard buffer). [b] Fluorescence quantum yield data. Estimated error: ±5%. [c] Hole arrival time ($\tau_a = k_a^{-1}$) and errors obtained from single-exponential fits to the main rise of the 525/575 nm ratio curve for **1A**−**4A** and **2AT**−**3AT** models, and from initial slopes for the other **nA** and **nAT** hairpins. [d] Estimated quantum yields and errors for hole trapping. The reported standard deviations are obtained from the results of three measurements for each sample. [e] Hole injection time ($\tau_i = k_i^{-1}$) and errors obtained from single-exponential fits to the rise of the 525/575 nm ratio curve for **H1**−**H3** models.

† Northwestern University.
‡ New York University.

10.1021/ja076876o CCC: $37.00

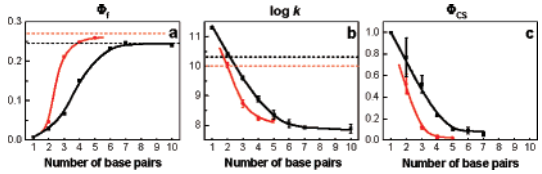

Figure 1. Fluorescence quantum yields (a), rate constants for hole arrival (b), and charge separation quantum yields (c) for hairpins **1A**−**7A**, **10A** (black squares), and **2AT**−**5AT** (red circles). In a and b, the fluorescence quantum yields and hole injection rate constants are displayed with black dashed lines for $\mathbf{H_1}$ and red dashed lines for $\mathbf{H_2}$.

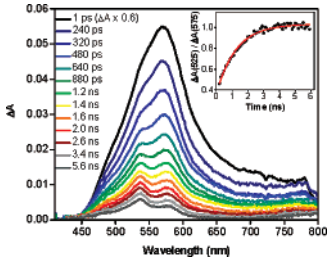

Figure 2. Transient absorption spectra of **3AT** at delay times of 1 ps to 5.6 ns following fs laser excitation at 350 nm. Inset: time-dependent 525/575 nm band intensity ratio for **3AT** and single-exponential fit to the data points (red curve).

Scheme 1. Kinetic Scheme for Fluorescence, Nonradiative Decay, Hole Injection, Hole Transport, Hole Trapping, and Charge Recombination in Hairpin **4A**

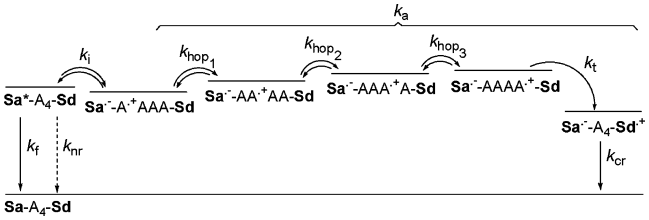

in Table 1 along with redetermined values for the **nA** hairpins, which are similar to those previously reported.[6,7]

Plots of the rate constants for hole arrival ($k_a = \tau_a^{-1}$) versus the number of base pairs separating Sa and Sd for the **nAT** and **nA** hairpins are shown in Figure 1b. The rate constants for hole injection in $\mathbf{H_1}$ and $\mathbf{H_2}$ ($k_i = \tau_i^{-1}$) are shown as horizontal dashed lines. The somewhat smaller value of k_i for $\mathbf{H_2}$ versus $\mathbf{H_1}$ and $\mathbf{H_3}$ plausibly reflects greater stabilization of the $Sa^{-\bullet}-A^{+\bullet}$ contact ion pair by an adjacent A versus T.[9] Except in the case of **1A**, values of k_a are comparable to or slower than k_i, in accord with a multistep hole hopping mechanism for charge separation (Scheme 1). Values of k_a are smaller for the **nAT** versus **nA** hairpins for all values of n, the difference being most pronounced for $n = 3$. Smaller values of k_a can account for the larger values of Φ_f for the **nAT** series (Figure 1a). Quantum yields for charge separation can be estimated by comparing the integrated band intensities of the transient absorption spectra with those for **1A** ($\Phi_{cs} = 1$). Values of Φ_{cs} for both the **nAT** and **nA** hairpins are summarized in Table 1, and plots of Φ_{cs} versus n are shown in Figure 1c. As is the case for k_a values, Φ_{cs} values are smaller for **nAT** versus **nA** hairpins, the most pronounced difference being observed for $n = 3$. For larger values of n, both Φ_{cs} and Φ_f are only weakly distance-dependent.

Notable features of these results are (a) the pronounced distance dependence of the fluorescence quantum yields, charge separation efficiency, and rate constants at short distances for both **nA** and **nAT** systems; (b) the weak distance dependence at longer distances for both systems; and (c) the decreased efficiencies and rate constants for hole arrival in the **nAT** versus **nA** systems. We previously attributed the change in the slope of a plot of k_a versus distance for **nA** hairpins (Figure 1b) to a change in mechanism from single-step superexchange at short distances to multistep hole hopping at longer distances.[7] The present data indicate that hopping is the dominant mechanism for hairpins having three or more intervening base pairs and perhaps even at shorter distances. The likely explanation for this distance dependence is Coulomb attraction between $Sa^{-\bullet}$ and holes residing on A in the **nA** or **nAT** bridge.[10] The Coulomb attraction is largest for the contact ion pair $Sa^{-\bullet}-A^{+\bullet}$ and decreases asymptotically as the distance between charges increases. Increasing energy of the bridge-oxidized state with increasing separation from $Sa^{-\bullet}$ should result in decreases in both the rate constant and quantum yield for hole arrival, which become smaller as the energy levels converge at longer distances (Scheme 1). Higher energy for the $A^{+\bullet}T$ versus $A^{+\bullet}A$ bridge-oxidized states can account for slower and less efficient hole transport via **nAT** versus **nA** sequences.

To our knowledge, the present study provides the first direct comparison of the dynamics and efficiency of photoinduced charge separation across **nAT** versus **nA** base pair sequences. Takada and co-workers have reported that quantum yield for charge separation between a naphthaldiimide hole donor and phenothiazine hole acceptor is larger for a 5A versus ATATA base pair sequence (0.014 vs 0.0039) by a factor of 3.6, similar to our result for **5AT** versus **5A**.[4] These workers have reported a similar preference for **nA** versus **nAT** sequences consisting of 7 or 20 base pairs.[5] Several groups have reported measurements of relative strand cleavage yields in duplexes having **nA** versus **nAT** sequences separating G, GG, or GGG hole traps.[2−5] Strand cleavage studies are based on charge shift reactions in which it is not necessary to overcome Coulomb attraction between oppositely charged radical ions. Thus it is not surprising that relatively small differences in efficiency for **nA** versus **nAT** bridges have been observed in strand cleavage studies.

Acknowledgment. This research is supported by the Office of Basic Energy Sciences, U.S. Department of Energy, under Contracts DE-FG02-96ER14604 (F.D.L.) and DE-FG02-99ER14999 (M.R.W.).

Supporting Information Available: Fluorescence decay data (Table S1), UV absorption spectra (Figures S1 and S4), fluorescence spectra (Figures S2, S3, and S5), transient absorption spectra for **2AT**, **4AT**, and **5AT** (Figures S6−S8), reference spectra for Sa*, $Sa^{-\bullet}$, and $Sd^{+\bullet}$ (Figure S9), and analysis of the transient spectra (S10). This material is available free of charge via the Internet at http://pubs.acs.org.

References

(1) (a) Schuster, G. B., Ed. *Long-Range Charge Transfer in DNA, I and II*; Springer: Berlin, 2004. (b) Wagenknecht, H. A. *Charge Transfer in DNA*; Wiley-VCH: Weinheim, Germany,2005.
(2) Giese, B.; Amaudrut, J.; Köhler, A.-K.; Spormann, M.; Wessely, S. *Nature* **2001**, *412*, 318−320.
(3) (a) Liu, C.-S.; Schuster, G. B. *J. Am. Chem. Soc.* **2003**, *125*, 6098−6102. (b) Shao, F.; Augustyn, K.; Barton, J. K. *J. Am. Chem. Soc.* **2005**, *127*, 17445−17452. (c) Williams, T. T.; Odom, D. T.; Barton, J. K. *J. Am. Chem. Soc.* **2000**, *122*, 9048−9049.
(4) Takada, T.; Kawai, K.; Cai, X.; Sugimoto, A.; Fujitsuka, M.; Majima, T. *J. Am. Chem. Soc.* **2004**, *126*, 1125−1129.
(5) Takada, T.; Kawai, K.; Fujitsuka, M.; Majima, T. *J. Am. Chem. Soc.* **2006**, *128*, 11012−11013.
(6) Lewis, F. D.; Zhu, H.; Daublain, P.; Cohen, B.; Wasielewski, M. R. *Angew. Chem., Int. Ed.* **2006**, *45*, 7982−7985.
(7) Lewis, F. D.; Zhu, H.; Daublain, P.; Fiebig, T.; Raytchev, M.; Wang, Q.; Shafirovich, V. *J. Am. Chem. Soc.* **2006**, *128*, 791−800.
(8) (a) Berlin, Y. A.; Kurnikov, I. V.; Beratan, D.; Ratner, M. A.; Burin, A. L. *Top. Curr. Chem.* **2004**, *237*, 1−36. (b) Conwell, E. M.; Bloch, S. M.; McLaughlin, P. M.; Basko, D. M. *J. Am. Chem. Soc.* **2007**, *129*, 9175−9181. (c) Jortner, J.; Bixon, M.; Langenbacher, T.; Michel-Beyerle, M. E. *Proc. Natl. Acad. Sci. U.S.A.* **1998**, *95*, 12759−12765.
(9) Voityuk, A. A.; Jortner, J.; Bixon, M.; Rösch, N. *Chem. Phys. Lett.* **2000**, *324*, 430−434.
(10) Private communication: F. C. Grozema and Y. A. Berlin.

JA076876O